



UPPSALA
UNIVERSITET

UPTEC F 19015

Examensarbete 30 hp
Januari 2019

2D Modelling of Phytoplankton Dynamics in Freshwater Lakes

Hugo Harlin



UPPSALA
UNIVERSITET

Abstract

2D Modelling of Phytoplankton Dynamics in Freshwater Lakes

Hugo Harlin

Teknisk- naturvetenskaplig fakultet
UTH-enheten

Besöksadress:
Angströmlaboratoriet
Lägerhyddsvägen 1
Hus 4, Plan 0

Postadress:
Box 536
751 21 Uppsala

Teléfono:
018 – 471 30 03

Telefax:
018 – 471 30 00

Hemsida:
<http://www.teknat.uu.se/student>

Phytoplankton are single celled organisms capable of photosynthesis, and are present in all the major oceans and lakes in the world. Phytoplankton contribute to 50% of the total primary production on Earth, and are the dominating primary producer in most aquatic ecosystems. This thesis is based on the 1D deterministic model by Jäger et. al. (2010) which models phytoplankton dynamics in freshwater lakes, where phytoplankton growth is limited by the availability of light and phosphorus. The original model is here extended to two dimensions to include a horizontal dimension as well as a vertical dimension, in order to simulate phytoplankton dynamics under varying lake bottom topographies. The model was solved numerically using a grid transform and a finite volume method in MATLAB. Using the same parameter settings as the 1D case studied by Jäger et. al. (2010), an initial study of plankton dynamics was done by varying the horizontal and vertical diffusion coefficients independently.

Handledare: Sebastian Diehl
Ämnesgranskare: Gunilla Kreiss
Examinator: Thomas Nyberg
ISSN: 1401-5757, UPTEC F19015

Populärvetenskaplig Sammanfattning

Phytoplankton är encelliga organismer kapabla till fotosyntes. De lever i alla världshav och sjöar, och bidrar till 50% av den totala primärproduktionen på jorden. Populationsdensiteten av phytoplankton är beroende av en rad faktorer som ljustillgång, närsalter, vattentemperatur, konsumption av andra organismer, etc. Vid rätta förhållanden kan phytoplankton reproduceras sig explosionsartat, en process som många känner till som 'algblooming'. Detta arbete bygger på den endimensionella phytoplanktonmodellen av Jäger et. al. (2010) som beskriver phytoplankton-dynamik i färskvattensjöar, där produktionen av alger är begränsat av tillgången på ljus och ett näringssämne (fosfor). Modellen generaliseras till två dimensioner för att studera effekten av horisontell diffusion och ett varierande sjö-djup. En finit-volym metod används för att implementera modellen i Matlab, och diffusions-koefficienter horisontellt och vertikalt varieras oberoende av varandra för att undersöka effekterna av den introducerade horisontella dimensionen.

Acknowledgements

I would like to thank my supervisor Sebastian Diehl at ICELAB Umeå University for his guidance and support, his engagement and feedback has been most appreciated. Further, I would like to thank my subject-supervisor Gunilla Kreiss at Uppsala University for her input on numerical issues and implementation, her expertise in numerical methods has been most help full. I would also like to thank Karl Larsson at Umeå University, who also helped me with issues related to the numerical method, and Mehdi Cherif for his thoughtful comments. Finally, I would like to thank everyone at ICELAB who contributed to an enjoyable work environment.

Contents

Abstract	ii
Populärvetenskaplig Sammanfattning	ii
Acknowledgements	iii
Table of Contents	iv
1 Introduction	1
1.1 Background	2
2 Theory	3
2.1 Reaction-advection-diffusion equation	4
2.2 The Model	5
2.3 Lake Geometry & Coordinate Transform	7
2.4 Boundary Conditions	8
3 Numerical Method - A Finite Volume Approach	10
3.1 Stiffness	14
3.2 Conservation of Nutrients	14
4 Results	15
5 Discussion	21
5.1 Sediment nutrient concentration	22
5.2 Finite Volume Method & Alternate Grid	23
5.3 Future Work	23
6 Conclusion	26
A Specific production and gross production	32

1 Introduction

The ability to accurately model ecosystems in nature has many applications. From a pure scientific standpoint, it is a useful tool which allows scientists to study the behavior of ecological systems and make predictions that further our understanding of the natural world, whereas the private sector can utilize models to increase yields or minimize costs [4, 33, 30]. Ecological models can also be used by governments and nongovernmental organizations (NGOs) for evidence based policy making, since they can be used to predict the impact of human activities on ecosystems [1, 3, 35, 39, 46, 43, 47, 48].

A contemporary example of an ecological catastrophe that could have been averted with ecological modelling is the modern salmon farming industry, which has had a substantial negative impact on its surrounding environment with the risk of disease spread and genetic pollution of native salmonid populations. Ford et. al.[15] use a general linear model in conjunction with a Ricker model [41] to study the survival of juvenile salmon in areas with salmon farming in Nova Scotia, Canada, and report that wild salmonid survival rate decreases of 50% are common in the presence of local salmon farming. Hindar et al. [22] use existing data from whole river experiments in Ireland and Norway to model the survival rates of wild salmon for varying amounts of escaped farmed salmon, and report that a recovery of the wild population is unlikely under all studied circumstances of previous salmon farming activity, even decades after the removal of salmon farms. While great damage has already been done to wild salmonid populations, ecological modelling has provided sound evidence of the negative consequences of salmon farming which can be used in future policy making to hinder further damage. This is but one example of where ecological modelling has been able to quantify the effects of human activity on its surrounding environment, and in order to proactively avoid similar situations in the future, such as the effects of global warming, ecological modelling is essential.

In this thesis a deterministic model of phytoplankton dynamics in freshwater lakes, developed by Jäger et al.[26], is implemented in two dimensions in order to study phytoplankton dynamics under varying bottom topographies. Algae exists as a free-floating mass that sinks with a constant rate and diffuses according to Ficks law [12].

The model itself consists of three coupled partial differential equations (PDE:s), see equations 3-5, that describe the algal density in the water, the dissolved nutrient density in the water, and the nutrient density in the sediment layer. It is assumed that growth of phytoplankton is limited by the availability of light and phosphorus, and that the diffusion coefficients are constants.

1.1 Background

Primary producers are organisms that rely on an external energy source, such as sunlight or the energy stored in inorganic chemical compounds, along with inorganic material to build organic molecules. Primary producers serve as a source of energy and organic compounds for all other organisms in an ecosystem, either directly through grazing or indirectly through predation, and are therefore vital for the continued existence of life [18, 24].

In terrestrial ecosystems the common primary producers are plants such as trees, shrubs, and grasses. Trees represent the vast majority of primary production in biomass, and microscopic producers such as algae account for only 7% of primary production on land [36].



Figure 1: High concentrations of phytoplankton of the coast of Finland is visible from space, photographed by a NASA satellite.

Source: "Phytoplankton and blue-green algae blooms.Finland_001" by [Seán Doran](#) is licensed under CC BY-NC-ND 2.0

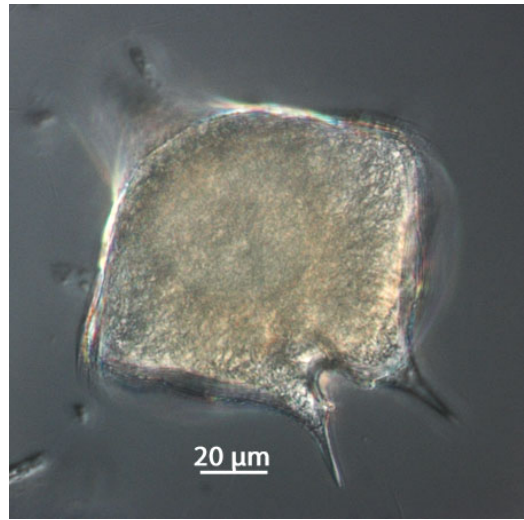


Figure 2: *Protoperidinium depressum*, a species of Dinoflagellate phytoplankton. It's appendages enables independent motion, an ability that is disregarded in this thesis.

Source: Photo by [Alexandra](#) is licensed under CC BY 3.0.

In aquatic environments however, the reverse is true and algae are key primary producers, they represent approximately 50% of the total primary production on Earth [29, 13]. The most common type of aquatic algae is called phytoplankton, which is a diverse group of microscopic autotrophic organisms where tens to hundreds of species can be found in a few milliliters of sea water [38]. Phytoplankton are very

small, invisible to the naked eye unless they are gathered in large quantities and appear as a green mass due to the presence of chlorophyll in the cells. Under the right conditions phytoplankton populations can increase very rapidly, a process commonly called an algal bloom. These blooms can cover large areas and are even visible from space in some cases, as can be seen in figure 1 which depicts high concentrations of phytoplankton of the coast of Finland.

Phytoplankton live freely suspended in water and sink very slowly due to their small size. Some groups, like the Euglenoids and the Dinoflagellates (figure 2), have appendages which enables independent motion [18], while others drift helplessly. In this thesis the assumption is made that algae does not possess any means of self propulsion.

In the real world, phytoplankton growth is limited by a multitude of abiotic factors depending on their geographical location such as water temperature [10], water salinity [40, 31, 5], nutrient availability [20, 19, 14, 50, 9], available light [21, 19], trace metals such as iron and zinc [21, 32, 42], et cetera. Biotic factors such as cell size [21] and microzooplankton grazing [7, 27] can also affect phytoplankton growth. Because of the importance of phytoplankton in aquatic ecosystems, the ability to accurately model phytoplankton dynamics is highly relevant and necessary to predict the impact of factors such as pollution, over-fertilization, and global warming on aquatic ecosystems.

2 Theory

There are two major types of models used to describe ecosystems: stochastic models and deterministic models. Stochastic models describe interactions in an ecosystem as random events that occur with a certain probability, and individual simulations can therefore differ even though the initial conditions are identical. Stochastic models are not restricted to modelling entire populations as a whole but can instead be expressed on an individual basis, where specimens in the same species are individually represented and interact with the environment and other individuals with some probability [2]. Stochastic models are often intuitive for this reason because they more closely mimic the interactions on an individual level compared to deterministic models.

The other major type of ecological models is deterministic models. Deterministic models are rigorously defined systems of differential equations that describe the rate of change of populations as a whole, and always yield the same solution given unchanged initial conditions. In contrast to stochastic models, deterministic models do not mimic individual interactions at all but instead try to emulate population

changes on a larger scale.

Since deterministic models are rigorously defined systems of equations with unique solutions, they can in simple cases be solved analytically. However, this is often impossible for more advanced models with complex geometry, and traditional numerical approaches for solving PDE:s such as finite differences or finite elements are used in practice.

2.1 Reaction-advection-diffusion equation

The model studied in this thesis is based on a well known equation called the reaction-advection-diffusion equation, which describes a system where two physical processes, advection and diffusion, as well as a reaction (source/sink) term, affect a modelled physical quantity. Written in a general form the reaction-advection-diffusion equation reads

$$\frac{\partial c}{\partial t} = \nabla(D\nabla c) - \nabla \cdot (\bar{v}c) + S \quad (1)$$

where c is the physical quantity (concentration of algae and dissolved nutrients in this thesis), D is the diffusion coefficient(s), \bar{v} is the velocity field that dictates advective motion, and S is a source/sink term. D is a matrix where the main diagonal is the diffusion coefficients in the axis directions, and the other elements are cross-terms. Diffusion is modelled according to Fick's Law of diffusion, which he derived experimentally in 1855 when studying the flux and change in concentration of salt diffusing through tubes between two reservoirs of water [12].

If diffusion is assumed to be constant in the coordinate directions, which is the case in the the 2D model studied in this thesis, the diffusion coefficient matrix becomes $D = \begin{bmatrix} d_x & 0 \\ 0 & d_z \end{bmatrix}$ where d_x and d_z are independent constants and x and z are the horizontal and vertical dimensions. Since the diffusion coefficients are not spatially dependent, one can rewrite the first term in equation 1 and yield

$$\frac{\partial c}{\partial t} = D\Delta c - \nabla \cdot (\bar{v}c) + S \quad (2)$$

where $\Delta = \left(\frac{\partial^2}{\partial x^2}, \frac{\partial^2}{\partial z^2} \right)$ is the spatial differential operator of the second order.

The reaction-advection-diffusion equation is very adaptable to a range of physical scenarios. Wertheim and Roose use it to model the transport of vascular endothelial growth factor C in the lymphatic system of zebra fish embryos [49]. The reaction-advection-diffusion equation is used under various names in the literature depending

on context, and the 'reaction' part of the name is often omitted for writing convenience. For example, in research related to electronics and semi-conductors the equation is commonly called the drift-diffusion equation, which alludes to the drift of electrons subject to an electric field. Horowitz uses the drift-diffusion equation to describe the electrical current in organic diodes [23]. The reaction-advection-diffusion equation can even be found in research on reinforcement learning: Pedersen et al. [37] use the equation to describe the choice process of a learning neural network, in order to better capture the complex nature of the choice process.

2.2 The Model

The model studied in this thesis was developed by Jäger et al.[26] and describes the dynamics of phytoplankton limited by access to light and a single nutrient (phosphorus) in a one dimensional body of water with finite depth. It is here implemented in two spacial dimensions, see equations 3 - 7 (parameters are listed in table 1), in order to study phytoplankton dynamics under varying bottom topographies and horizontal motion. The lake was assumed to be symmetric around its deepest point and thus half of the lake was simulated, see section 2.3 for further details.

The added horizontal dimension is denoted by x . The vertical dimension is denoted by z and faces downward, so that the sinking velocity of algae is positive in the z -direction. The concentration of phytoplankton is denoted by the variable A which is a function of time and space $A = A(x, z, t)$, and algae sink with a constant velocity v in the positive z direction which points downward. The change of phytoplankton concentration in $mgCm^{-3}$ is given by equation 3. Algae diffuses both vertically and horizontally with independent diffusion coefficients d_x and d_z .

$$\frac{\partial A}{\partial t} = (G(R, I) - l)A - v \frac{\partial A}{\partial z} + d_x \frac{\partial^2 A}{\partial x^2} + d_z \frac{\partial^2 A}{\partial z^2} \quad (3)$$

$$\frac{\partial R}{\partial t} = -q((G(R, I) - l)A) + d_x \frac{\partial^2 R}{\partial x^2} + d_z \frac{\partial^2 R}{\partial z^2} \quad (4)$$

$$\frac{\partial R_s}{\partial t} = -rR_s + qvA(z_{max}(x)), \{z_{max}(x) = max(z)|_x\} \quad (5)$$

$$I(z) = I_0 \exp \left(-k \int_0^z A(s, t) ds - k_{bg} z \right) \quad (6)$$

$$G(R, I) = G_{max} \frac{R}{M_L + R} \frac{I}{H_L + I} \quad (7)$$

The model assumes that the limiting factors to the growth of algae is the availability of phosphorus R , and the available light I , which is dependent on depth

$I = I(z)$. The change in phosphorus concentration in $mgPm^{-3}$ with respect to time is given by equation 4, where R is a function of space and time in the same manner as the concentration of phytoplankton A, $R = R(x, z, t)$.

The ratio of nutrient to algal carbon content (stoichiometry) is a fixed value q called the Redfield ratio, an empirical value derived from measurements on marine water samples by Redfield in 1934 [11]. The Redfield ratio is commonly expressed as proportions of carbon, nitrogen, and phosphorus by atoms, C:106 — N:16 — P:1. Multiplying the P/C ratio with the molecular weight of carbon (31u) and phosphorus (12u) yields the constant $q = 0.0244$ used in this thesis. In real life phytoplankton have the ability to adjust the nutrient-carbon ration in the cell depending on nutrient abundance, and differs among different phytoplankton species. It is here assumed that algae have no such ability.

The growth of the algae is governed by the product of two Monod equations in equation 7 , where I is the light intensity at the given depth z and is described by Beer-Lambert's law in equation 6 where I_0 is the intensity at the surface [34, 45]. The two parameters M_L and H_L in equation 7 are half saturation constants for the nutrients and light respectively, and they denote the nutrient concentration and light intensity at which the production of algae is at half of its maximal capacity given no other resource restraints.

The algae hinder light from penetrating the water, which is modelled with a light-attenuation coefficient k , and any background light attenuation caused by other substances than phytoplankton is modelled with the coefficient k_{bg} . Algae concentration is also affected by maintenance respiration losses, modelled with a constant rate l .

The death of phytoplankton cells is modelled with two mechanisms: respiration and the interaction with the sediment. Dead algal cells are not explicitly represented with a state variable, and alive cells either respire until they disappear, or sink until they reach the sediment and are instantly turned into sedimented nutrients.

The limiting nutrient (phosphorus) exists in two forms: in dissolved mineral form in the water mass, denoted by the variable R and described by equation 4, or bound in a one dimensional sediment layer at the bottom of the lake, denoted by Rs in equation 5. When in the dissolved state the nutrients diffuse with the same diffusion coefficients as the algae, but they do not sink. The nutrients at the bottom of the lake are remineralized into the water at a rate r . Algae cannot access the nutrients in the sediment directly in order to grow, and sedimented nutrients have to remineralize into water first in order to be accessed by phytoplankton.

Table 1: Parameters and state variables

Quantity	Definition	Value/Range	Unit
A_j	Phytoplankton concentration	10*	mg C m^{-3}
R	Nutrient concentration	10*	mg P m^{-3}
R_s	Sedimented nutrient density	100*	mg P m^{-2}
I	Light intensity	300	$\mu \text{ mol photons m}^{-2} \text{ s}^{-1}$
l_{bg}	Background mortality	.2	day^{-1}
v	Sinking speed	0.25	m day^{-1}
d_x	Horizontal turbulent diffusion coefficient	[1, 1000]	$\text{m}^2 \text{ day}^{-1}$
d_z	Vertical turbulent diffusion coefficient	[1, 1000]	$\text{m}^2 \text{ day}^{-1}$
q	Algal nutrient quota (Redfield ratio [11])	.0244	R C^{-1}
r	Specific mineralization rate of sedimented nutrients	.02	day^{-1}
G_{max}	Maximum specific algal production	1.08	day^{-1}
M_L	Nutrient uptake half-saturation constant	1.5	mg R m^{-3}
H_L	Light uptake half-saturation constant	1.0	$\mu \text{ mol photons m}^{-2} \text{ s}^{-1}$
I_0	Light intensity at surface	1400	$\mu \text{ mol photons m}^{-2} \text{ s}^{-1}$
k	Algal light attenuation coefficient	.0003	$\text{m}^2 \text{ mg C}^{-1}$
k_{bg}	Background light attenuation coefficient	.4	m^{-1}
l	Specific algal maintenance respiration losses	.1	m^{-1}
L_{max}	Maximum water column depth	50	m
L_{min}	Minimum water column depth	0.1	m
W	Half lake width	50	m
x	Horizontal coordinate	-	m
z	Vertical coordinate	-	m
α	lake bottom slope exponent	1	-

* Initial values

2.3 Lake Geometry & Coordinate Transform

The geometry of the lake was devised so that the lake bottom varied from L_{max} at the center, to L_{min} at the shore with slope α , see figure 3. The exponent α allows for a variable slope of the lake bottom, with $\alpha = 0$ corresponding to a flat bottom with a uniform depth L_{max} , and $\alpha = 1$ corresponds to a linear slope. The transform from the original coordinate system to a Cartesian system is given by equations 8 and 9

$$z = \frac{\eta}{Z_n} \left(L_{max} + (L_{min} - L_{max}) \left(\frac{\xi}{X_n} \right)^\alpha \right), \alpha \in \mathbb{R} \quad (8)$$

$$x = W\xi \quad (9)$$

$$\xi \in [0, X_n], \eta \in [0, Z_n]$$

where X_n and Z_n are the number of mesh grid nodes in the horizontal and vertical dimension respectively.

Generally, for a coordinate transform to be valid when using a finite volume method it should be bijective, meaning that no two points in the original system are mapped to the same point in the transformed system and vice versa, a one-to-one correspondence. This is because the finite volume method uses distances between

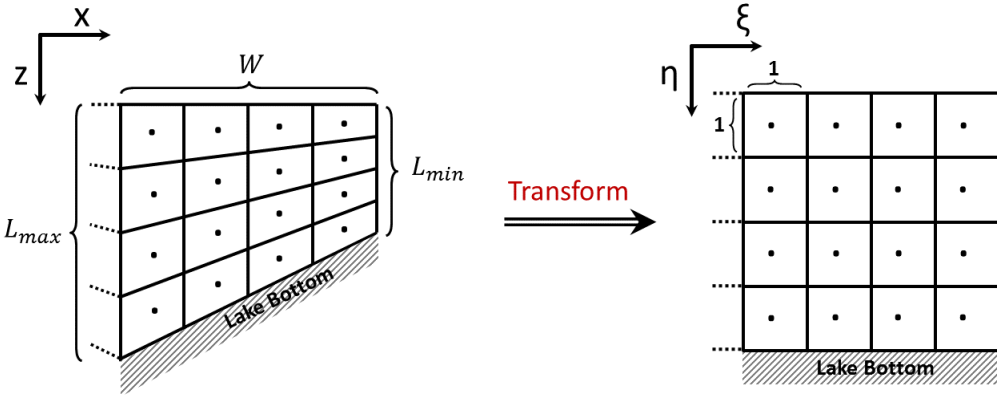


Figure 3: Original Lake mesh geometry and the transformed Cartesian mesh. Lake depth varied from $z_{max} = 50m$ at the center to $z_{min} = 0.1m$ at the shore, a linear slope was used for all simulations. Half the lake was simulated under the assumption of symmetry at the lake center. A grid centered finite volume method was used, meaning that the state variables were defined in the center of each grid cell.

nodes when calculating the flows in and out of each grid cell, and if grid nodes overlap expressions risk becoming undefined resulting in failure. For this reason one should not set the parameter L_{min} to zero, since this would mean that all nodes on the shallow edge of the lake would converge on the same point at the surface. For the special case of the boundary conditions used in this thesis however, L_{min} can be allowed to be zero because the flows out of the sides of the lake is assumed to be zero, and thus the terms relating to the zero length boundary of the edge nodes can be set to zero without evaluating undefined terms. This was not done because future studies of the model might include boundary conditions that allow for a non-zero flux at the left and right edges, and the grid was chosen to facilitate cases such as these. Note however that a finite volume method does not require a Cartesian mesh at all and different geometric shapes can be used interchangeably, such that the lake depth can be set to zero without overlapping nodes (see section 5.2 of the discussion for more details).

2.4 Boundary Conditions

In this thesis the model lake is assumed to be symmetric and therefore simulations are run on one half, with the left border of the computation grid corresponding to the center of the lake. Boundary conditions are formulated such that no nutrients leak out of the lake, and such that the above assumption of symmetry holds. Formulating

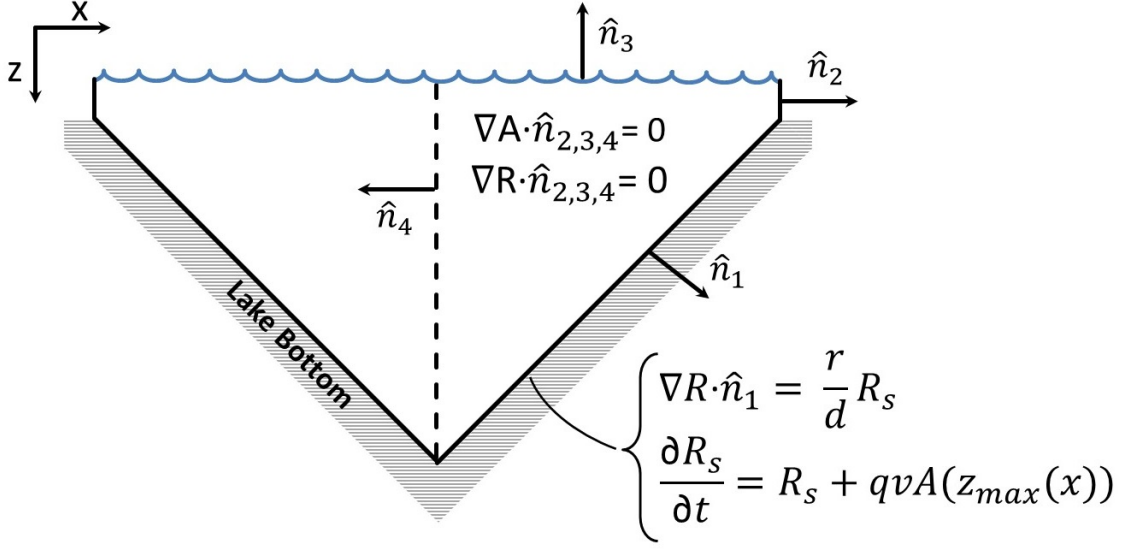


Figure 4: Lake symmetry and boundary conditions. Half the lake is simulated under the assumption of symmetry along the center dotted line. This assumption gives rise to the boundary conditions $\nabla R \cdot \hat{n}_4 = 0$, $\nabla A \cdot \hat{n}_4 = 0$. At the surface and lake sides the assumption is made that the nutrient flux is zero. At the bottom of the lake algae sink into the sediment and instantly become sedimented nutrients, according to the equation 13 where $z_{max}(x)$ returns the maximal depth $\max(z)$ for a given horizontal coordinate x . Sedimented nutrients remineralize into the lake as dissolved nutrients according to equation 11.

these criteria into equations yield

$$\nabla R \cdot \hat{n}_{2,3,4} = 0 \quad (10)$$

for the dissolved nutrients R on the top, left, and right grid boundaries where \hat{n} is the outward facing normal, see figure 4. At the bottom of the lake a remineralization process takes place where the sediment releases nutrients back into the water in a dissolved state. This process is modelled with the boundary condition

$$\nabla R \cdot \hat{n}_1 = \frac{r}{d} R_s \quad (11)$$

where \hat{n}_1 is the outward facing normal of the lake bottom. The boundary conditions for the algae are similar to the dissolved nutrients R , except that algae that have sunk to the bottom die and are converted into sediment. This yields

$$\nabla A \cdot \hat{n}_{2,3,4} = 0 \quad (12)$$

for the top, left, and right borders where $\hat{n}_{2,3,4}$ are the corresponding outward facing normal vectors. The rate of change of the nutrients in the sediment is affected by sinking algae becoming sedimented nutrients and a remineralization process where nutrients bound in the sediment are released back into the lake as dissolved nutrients,

$$\frac{\partial R_s}{\partial t} = -rR_s + qvA(z_{max}(x)), \quad (13)$$

where $z_{max}(x)$ returns the maximal depth $\max(z)$ for a given horizontal coordinate x , $z_{max}(x) = \max(z)|_x$.

3 Numerical Method - A Finite Volume Approach

A cell centered finite volume method was used in conjunction with a coordinate transform to numerically simulate the model in MATLAB. The finite volume method is based on defining the rate of change of a control volume in the computation domain, and relating that change to the net flux on the borders with Gauss' divergence theorem. This means that the net flow out of a grid cell is equal to the flow from that cell into the surrounding cells, and thus the method is inherently conservative and thus suitable for this model.

Integrating equation 3 over a control volume Ω (fig 5) yields:

$$\iint_{\Omega} \frac{\partial A}{\partial t} \partial x \partial y = \iint_{\Omega} \left((G(R, I) - l)A - v \frac{\partial A}{\partial z} + d_x \frac{\partial^2 A}{\partial x^2} + d_z \frac{\partial^2 A}{\partial z^2} \right) \partial x \partial y. \quad (14)$$

Since the spatial and temporal variables are independent, we can move the time differentiation outside the integral on the left hand side. Using cell centered quadrature to evaluate the l.h.s. integral, we get

$$C \frac{\partial A}{\partial t} = \iint_{\Omega} \left((G(R, I) - l)A - v \frac{\partial A}{\partial z} + d_x \frac{\partial^2 A}{\partial x^2} + d_z \frac{\partial^2 A}{\partial z^2} \right) \partial x \partial y \quad (15)$$

where C is the area of the control volume Ω . The next step is to separate the right hand side integral into source/sink terms and spatial terms,

$$C \frac{\partial A}{\partial t} = \iint_{\Omega} (G(R, I) - l)A \partial x \partial y + \iint_{\Omega} \left(-v \frac{\partial A}{\partial z} + d_x \frac{\partial^2 A}{\partial x^2} + d_z \frac{\partial^2 A}{\partial z^2} \right) \partial x \partial y. \quad (16)$$

We evaluate the source/sink term integral in the same way as the l.h.s. integral, using cell centered quadrature.

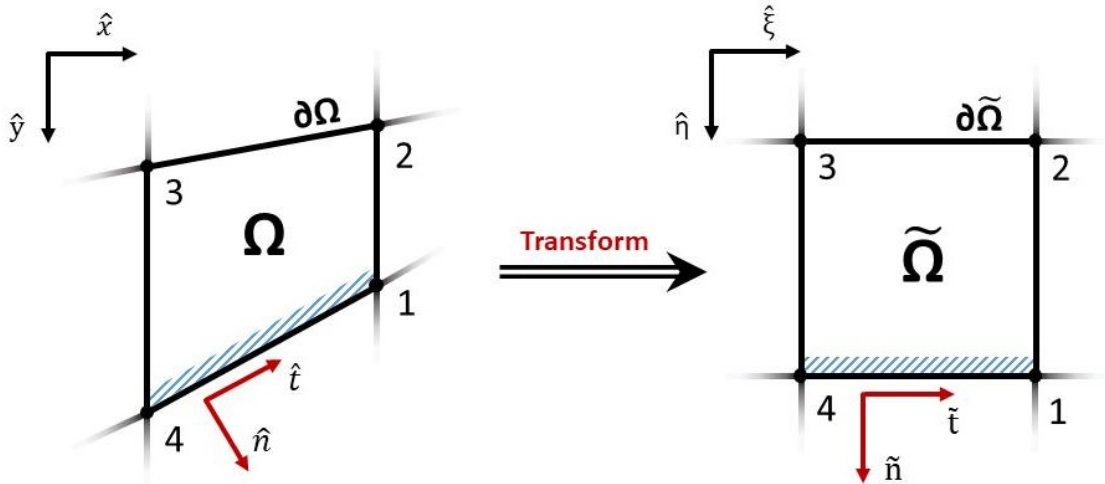


Figure 5: Control volume Ω in the original space to the left, and in the transformed space to the right where it is noted as $\tilde{\Omega}$. $\partial\Omega$ and $\partial\tilde{\Omega}$ signifies the boundaries of the control volumes in the original and transformed coordinate spaces respectively. The bottom side marked in blue is the last of the four line integrals of the r.h.s. of equation 24. The algae concentration A and nutrient concentration R was defined in the middle of each grid cell, a so-called cell centered finite volume method was used.

$$C \frac{\partial A}{\partial t} = C(G(R, I) - l)A + \iint_{\Omega} \left(-v \frac{\partial A}{\partial z} + d_x \frac{\partial^2 A}{\partial x^2} + d_z \frac{\partial^2 A}{\partial z^2} \right) \partial x \partial y. \quad (17)$$

At this point the divergence theorem is applied to the remaining integral,

$$\frac{\partial A}{\partial t} = (G(R, I) - l)A + \frac{1}{C} \oint_{\partial\Omega} \left(-vA + d_x \frac{\partial A}{\partial x} + d_z \frac{\partial A}{\partial z} \right) \hat{n} ds, \quad (18)$$

where $\partial\Omega$ is the border of the control volume, see figure 5, and \hat{n} is the outward facing normal integrating in the counter clockwise direction. We express the remaining integral in matrix notation in preparation for transformation

$$I = \oint_{\partial\Omega} (-\hat{v}A + D\nabla A) \hat{n} ds, \quad (19)$$

where $D = \begin{bmatrix} d_x & 0 \\ 0 & d_z \end{bmatrix}$ is the matrix of diffusion coefficients, $\hat{v} = \begin{bmatrix} 0 \\ v \end{bmatrix}$ is the velocity field dictating algal sinking and $\nabla = \begin{bmatrix} \partial/\partial x \\ \partial/\partial z \end{bmatrix}$ is the spatial differential operator. Instead of computing the integral directly, we transform our domain Ω into a Cartesian grid

with unit spacing. To achieve this we need to relate operators and differentials in our original domain to our new domain. Starting with the normal vector \hat{n} , we have

$$\hat{n} = \frac{1}{\|J^{-T}\tilde{n}\|} (J^{-T}\tilde{n}) \quad (20)$$

where \tilde{n} is the transformed normal vector and J is the jacobian of the coordinate transform,

$$J = \begin{bmatrix} \partial x / \partial \xi & \partial x / \partial \eta \\ \partial z / \partial \xi & \partial z / \partial \eta \end{bmatrix}, \quad (21)$$

where $\partial x / \partial \eta = 0$ for the transform used in this thesis. The differential ds becomes

$$ds = \|J\tilde{t}\| d\tilde{s}, \quad (22)$$

where \tilde{t} is a vector of unit length pointing in the integration direction in the transformed space. Next we express the nabla operator in our new coordinates:

$$\nabla = J^{-T} \tilde{\nabla}, \quad (23)$$

where $\tilde{\nabla} = \begin{bmatrix} \partial / \partial \xi \\ \partial / \partial \eta \end{bmatrix}$ is the differential operator in the transformed space.

Finally, we can express the remaining integral in the transformed coordinate system

$$I = \oint_{\partial\tilde{\Omega}} \frac{1}{\|J^{-T}\tilde{n}\|} (J^{-T}\tilde{n})^T (-\tilde{v}A + DJ^{-T}\tilde{\nabla}A) \|J\tilde{t}\| d\tilde{s} \quad (24)$$

Since the coordinate transform is analytic, we can write an analytic expression for the Jacobian matrix and simplify the integral before using numerical methods for evaluating the integral. We split the line integral into four parts, one for each side of the square transformed control volume (figure 5), and numerically approximate each integral individually using conventional integral approximations.

Below is an in detail derivation of the resulting implemented expression for the integral along the bottom of the transformed control volume. The remaining three integrals where derived and approximated in the same way, the only difference being the normal and tangential vectors \tilde{n} and \tilde{t} . Integrating from node 4 to node 1 in the transformed control volume $\tilde{\Omega}$ (figure 5) we have:

$$I_{4 \rightarrow 1} = \int_{\xi_4}^{\xi_1} \frac{1}{\|J^{-T}\tilde{n}\|} (J^{-T}\tilde{n})^T (-\bar{v}A + DJ^{-T}\tilde{\nabla}A) \|J\tilde{t}\| d\xi \quad (25)$$

where

$$\left\{ \begin{array}{l} \tilde{n} = \begin{bmatrix} 0 \\ 1 \end{bmatrix}, \tilde{t} = \begin{bmatrix} 1 \\ 0 \end{bmatrix}, \bar{v} = \begin{bmatrix} 0 \\ v \end{bmatrix} \\ D = \begin{bmatrix} d_x & 0 \\ 0 & d_z \end{bmatrix}, J = \begin{bmatrix} \partial x / \partial \xi & 0 \\ \partial z / \partial \xi & \partial z / \partial \eta \end{bmatrix} \quad \{\partial x / \partial \eta = 0 \text{ due to transform}\} \\ \frac{J^{-T} \tilde{n}}{\|J^{-T} \tilde{n}\|} = \frac{1}{\sqrt{\frac{\partial x^2}{\partial \xi^2} + \frac{\partial z^2}{\partial \xi^2}}} \begin{bmatrix} -\frac{\partial z}{\partial \xi} \\ \frac{\partial x}{\partial \xi} \end{bmatrix} \left\{ \frac{\partial x}{\partial \xi} = \left| \frac{\partial x}{\partial \xi} \right|, \frac{\partial z}{\partial \eta} = \left| \frac{\partial z}{\partial \eta} \right| \right\} \\ -\bar{v} A = \begin{bmatrix} 0 \\ -v A \end{bmatrix} \\ D J^{-T} \tilde{\nabla} A = \frac{1}{\frac{\partial x}{\partial \xi} \frac{\partial z}{\partial \eta}} \begin{bmatrix} d_x \left(\frac{\partial z}{\partial \eta} \frac{\partial A}{\partial \xi} - \frac{\partial z}{\partial \xi} \frac{\partial A}{\partial \eta} \right) \\ d_z \frac{\partial x}{\partial \xi} \frac{\partial A}{\partial \eta} \end{bmatrix} \\ \|J \tilde{t}\| = \sqrt{\frac{\partial x^2}{\partial \xi^2} + \frac{\partial z^2}{\partial \xi^2}} \end{array} \right.$$

Insertion in equation 25 yields:

$$I_{4 \rightarrow 1} = \int_{\xi_4}^{\xi_1} \frac{1}{\sqrt{\frac{\partial z^2}{\partial \xi^2} + \frac{\partial x^2}{\partial \xi^2}}} \begin{bmatrix} -\frac{\partial z}{\partial \xi} \\ \frac{\partial x}{\partial \xi} \end{bmatrix}^T \left(\begin{bmatrix} 0 \\ -v A \end{bmatrix} + \frac{1}{\frac{\partial x}{\partial \xi} \frac{\partial z}{\partial \eta}} \begin{bmatrix} d_x \left(\frac{\partial z}{\partial \eta} \frac{\partial A}{\partial \xi} - \frac{\partial z}{\partial \xi} \frac{\partial A}{\partial \eta} \right) \\ d_z \frac{\partial x}{\partial \xi} \frac{\partial A}{\partial \eta} \end{bmatrix} \right) \sqrt{\frac{\partial x^2}{\partial \xi^2} + \frac{\partial z^2}{\partial \xi^2}} d\xi \quad (26)$$

Simplification yields:

$$I_{4 \rightarrow 1} = \int_{\xi_4}^{\xi_1} \left(-v A \frac{\partial x}{\partial \xi} + \frac{1}{\frac{\partial x}{\partial \xi} \frac{\partial z}{\partial \eta}} \left(d_x \left(\frac{\partial z^2}{\partial \xi} \frac{\partial A}{\partial \eta} - \frac{\partial z}{\partial \xi} \frac{\partial z}{\partial \eta} \frac{\partial A}{\partial \xi} \right) + d_z \frac{\partial x^2}{\partial \xi} \frac{\partial A}{\partial \eta} \right) \right) d\xi \quad (27)$$

Rearranging diffusion terms in preparation for integral evaluation:

$$I_{4 \rightarrow 1} = \int_{\xi_4}^{\xi_1} \left(-v A \frac{\partial x}{\partial \xi} + \frac{\partial A}{\partial \eta} \frac{1}{\frac{\partial x}{\partial \xi} \frac{\partial z}{\partial \eta}} \left(d_x \frac{\partial z^2}{\partial \xi} + d_y \frac{\partial x^2}{\partial \xi} \right) - d_x \frac{\partial A}{\partial \xi} \frac{\partial z}{\partial \xi} \frac{\partial x}{\partial \xi}^{-1} \right) d\xi \quad (28)$$

A cell centered finite volume method was used in this thesis, which means that phytoplankton concentration A and dissolved nutrient concentration R is defined in the middle of each grid cell. The integral 28 was evaluated using the midpoint rule, and the terms $\frac{\partial A}{\partial \xi}$ and $\frac{\partial A}{\partial \eta}$ were evaluated in the middle of the integration interval with finite differences using the neighbouring grid cells. Since the transform analytic, the

terms $\frac{\partial z}{\partial \eta}$, $\frac{\partial z}{\partial \xi}$, $\frac{\partial x}{\partial \eta}$, $\frac{\partial x}{\partial \xi}$ are defined everywhere and were thus evaluated in the middle of the integration interval. The finite volume formulation of equation 4 was done in the same way as the case of the algae A, the only difference being the absence of an advection term and the differing source term. With explicit expressions for the time derivative of our quantities A, R , and R_s , we can write the whole system in matrix form as

$$\frac{\partial \bar{x}}{\partial t} = M\bar{x} \quad (29)$$

where \bar{x} is a vector of the state variables A , R , and R_s , and M is the matrix form of the integral approximations described above. To solve the system of equations in time, the built in MATLAB function ODE15s was used, which is a variable order method that is suitable for stiff systems of equations, see section 3.1 below. A callback was used to stop the simulation when the norm of the matrix $\partial A / \partial t$ was smaller than 10^{-5} .

3.1 Stiffness

Stiffness is a property of a differential equation or system of differential equations, and can loosely be defined as a high sensitivity to the step size where the inaccuracy of the numerical solution is large unless the step size is taken to be very small. Normally, one would expect that if the solution of the equation in question is smooth with small gradients, then a relatively larger step size can be used as opposed to a solution that varies sharply. This is often the case, but interestingly this does not apply all the time. There are equations that require extremely small time-steps to achieve an accurate solution, even when the analytic solution displays smooth behavior. For physical systems such as the one studied in this thesis, stiffness can arise when the time scales of different physical processes vary greatly[6]. This showed to be the case when simulated with low values of the diffusion coefficients, which coincides well with the above statement since this implies that for low values of the diffusion coefficients the diffusion induced movement is on a much slower time-scale than movement caused by sinking.

3.2 Conservation of Nutrients

An important property of the numerical method is the absence of numerical sinks or sources. Nutrients in the lake can move physically and be either bound in algae (A), free floating as dissolved nutrients (R), or bound in the sediment (R_s), but the

total amount of nutrients in interior of the lake should not change with time if there is no net flux at the lake borders. There can however be a flux of nutrients at the boundary given the appropriate boundary conditions, in which case the total nutrient content can fluctuate, but the numerical method itself should not give rise to any nutrient sources or sinks. Formally, one can define the conservation of nutrients in the internal of the lake as

$$0 = \frac{\partial}{\partial t} \left(\sum_i a_i (q * A_i + R_i) \right) \quad (30)$$

where the sum over i signifies all cells in the mesh, a_i the area of cell i , and A_i, R_i are the concentrations at the center of each cell. The finite volume method used in this thesis was chosen because it is inherently conservative and satisfies the conservation criteria above. In contrast, a finite difference method, which was used initially, will always exhibit leaks/sources for a non-cartesian 2D domain and is thus only suitable for rectangular grids.

4 Results

The introduction of a second dimension to the model by Jäger et. al. [26] allows for horizontal diffusion to affect phytoplankton dynamics, and introduces varying water depths that phytoplankton can inhabit. To study the effects of a second dimension and horizontal diffusion, the model was run to steady state with all parameters fixed except the diffusion coefficients which were varied independently in the interval range $(1, 10, 100, 1000) \text{ m}^2 \text{ day}^{-1}$ in order to compare results to the work of Jäger et. al.[26], and the fixed parameters where set to the same values as [26]. The results from these simulations can be seen in figures 6 - 8 and tables 2 - 4, see table 1 for numerical values of the fixed parameters. A callback function was used to detect steady state, where the simulation was stopped when the 2-norm of the matrix $\frac{\partial A}{\partial t}$ was smaller than 10^{-5} .

Comparing results to the work by [26], the 2D model never exhibits total extinction of algae at any point in the lake, whereas the 1D model exhibits total extinction for a vertical diffusion coefficient of 100 and $1000 \text{ m}^2 \text{ day}^{-1}$, and depths greater than 45 and 32m respectively. Even for low horizontal diffusion and high vertical diffusion, figure 6 plot D_2 , algae is present everywhere in the two dimensional case. While the vertical dynamics at those particular depths are the same in the 1D and 2D model, the presence of horizontal diffusion in the 2D model enables algae from neighbouring, shallower depths to propagate into the deeper regions. This effect is greater the

higher the horizontal diffusion coefficient is, and this behavior can be clearly seen in figure 6 when comparing plot A_2 and M_2 where the concentration of algae in M_2 is higher at the deeper parts of the lake compared to A_2 .

In general, there seems to be stronger trends when the vertical diffusion coefficient d_z is varied compared to d_x . For example, the proportion of nutrients bound in sediment changes with two orders of magnitude as d_z ranges from 1 to 1000, see table 4, whereas changes were generally much smaller for varying values of d_x where the greatest difference was found when comparing the proportion of dissolved nutrients for $d_z = 1000$ and $d_x = 1, 1000$ with a one order of magnitude increase. For all simulated cases the majority of the total nutrients in the system is bound in either the sediment or is in a dissolved state, and the highest concentration of algae is 16.3% for $d_x = 1000$ and $d_z = 1$, see table 2. For low vertical diffusion a majority of nutrients is in a dissolved state as can be seen in table 4, and decreases sharply as the horizontal diffusion increases. When the vertical diffusion approaches zero, all nutrients will end up as dissolved nutrients at steady state. This is because the vertical diffusion is the only transport mechanism that enables algae to propagate upwards in the water, and if the vertical diffusion is removed the algae will simply sink to the bottom and turn into sedimented nutrients. The sediment will in turn remineralize as dissolved nutrients, eventually depleting completely resulting in 100% dissolved nutrients. This trend can clearly be seen in table 3, where the proportional dissolved nutrient content increases as d_z decreases. To simulate a scenario with no vertical diffusion is challenging however, since for very low values of d_z the model becomes very stiff (see section 3.1 in section 3), and the method used in this thesis fails to achieve an accurate solution.

A shared behavior of all simulations is the concentration of sedimented nutrients in the shallow regions, see plots A_1-L_1 in figure 6. The spacial distribution of the sediment is unimodal for all simulations, and the highest concentration of sedimented nutrients is located at the far left edge of the lake except for the cases C_1 and D_1 where $d_x = 1$ and $d_z = 100, 1000$ respectively, here the nutrient concentration in the sediment peaks at an approximate depth of 10m. At first glance this general behavior of the majority of the sedimented nutrients in the shallows might seem counter-intuitive, since the opposite is true in real lakes where sediment congregates in the deepest parts [16]. This discrepancy is due to several factors: in the model, once nutrients are bound in the sediment, there is no mechanism that transports them horizontally and they either stay inert or remineralize as dissolved nutrients. In real lakes, turbulence along the bottom resuspend sediment particles into the water, and since these sink this results in sedimented particles being transported into the deeper parts, a phenomenon that the model cannot emulate. This discrepancy is discussed

in section 5.1 of the discussion.

Two other factors that causes high concentrations of nutrients in the sediment is the water column depth and specific production G . In figure 7 the specific production of select simulations can be seen. The optimal zone of growth for the algae is near the surface where the availability of light is the highest while there is also access to nutrients. The generic pattern of the optimal growth zone being horizontally distributed and situated close to the surface is common for all the simulations. While the influx of light is highest at the surface, nutrient concentrations increase with depth and is greatest at the bottom. This means that remineralized nutrients from the deep parts of the lake have to diffuse a greater length to reach the habitable zone of the phytoplankton compared to remineralized nutrients in shallow areas. Thus, specific production is generally lower for deeper water columns which can be seen in figure 7.

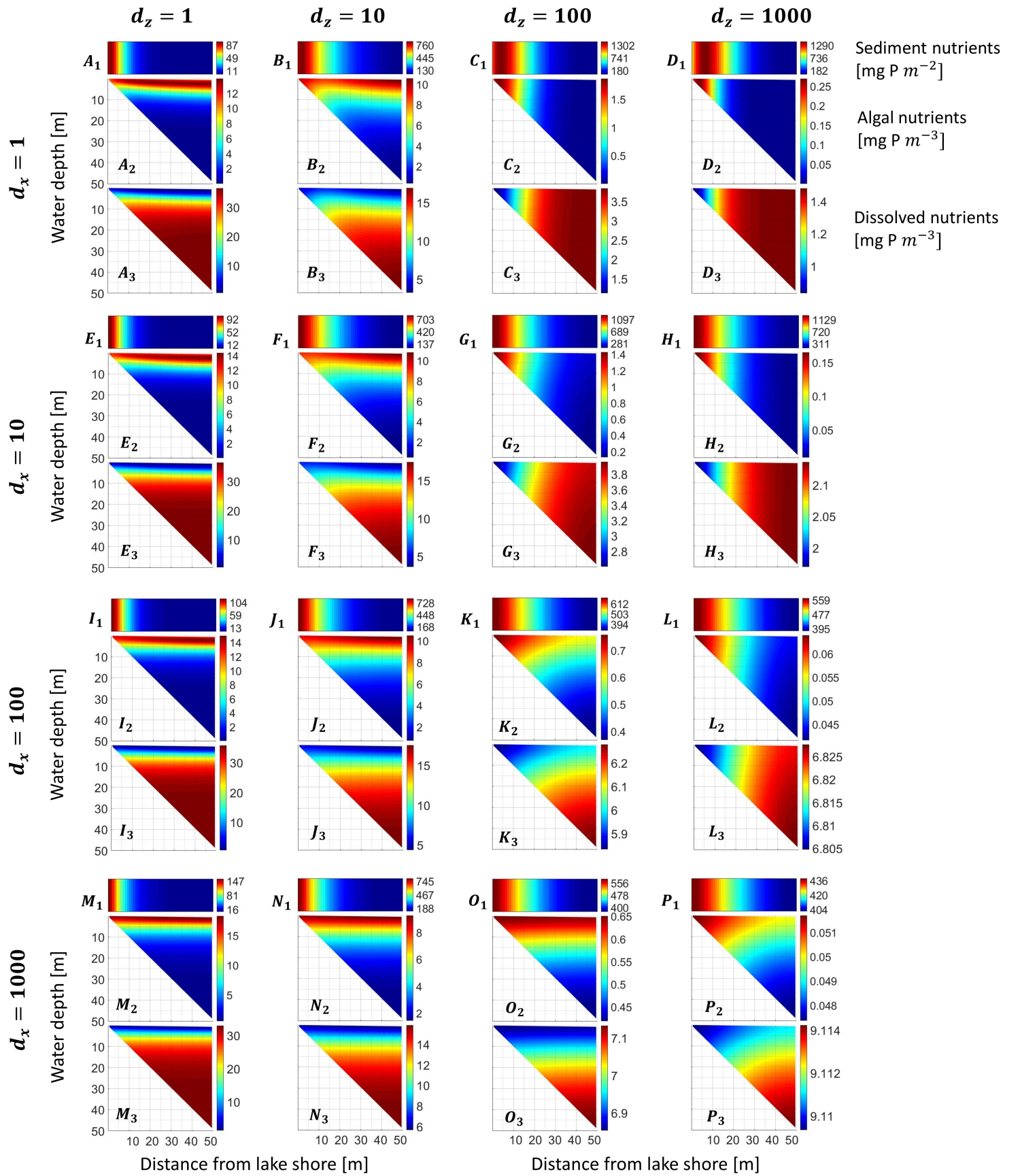


Figure 6: Phytoplankton, dissolved nutrient, and sediment nutrient content at steady state for varying diffusion coefficients. All parameters were kept constant except the diffusion coefficients, see table 1 for numerical values. The x-axes corresponds to the distance from the lake center (right border), and the y-axis corresponds to water depth. The diffusion coefficients were varied independently with values 1, 10, 100, and $1000 \text{ m}^2\text{day}^{-1}$. The plots are grouped and numbered such that X_1 is the nutrient content in the sediment, X_2 is the nutrient concentration bound in algae, and X_3 is the concentration of dissolved nutrient and all plots X_n correspond to the same set of parameters. Note that the color bars are scaled individually for each plot, so while the same qualitative pattern is present in both H_2 and C_2 for example, the concentration of nutrient in C_2 is much higher.

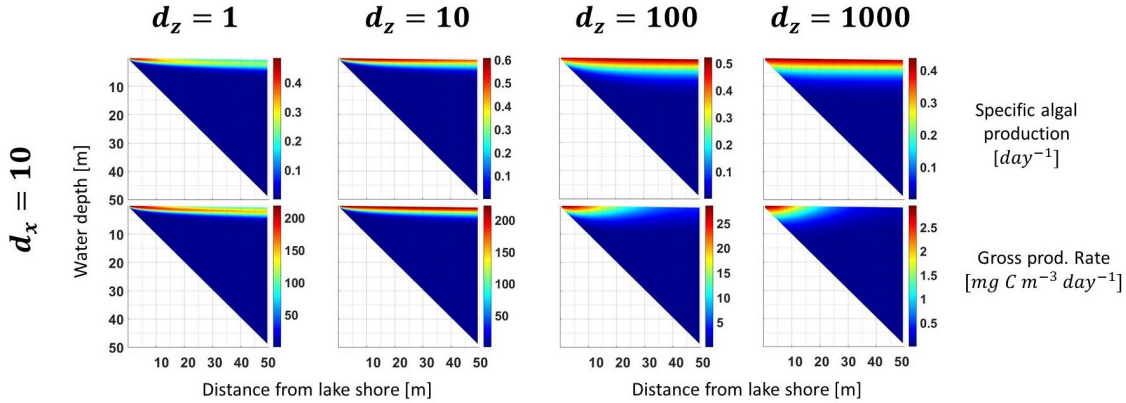


Figure 7: Specific algal production (G) and gross production rate (G^*A) for $d_x = 10$ and $d_z = 1, 10, 100, 1000$. The horizontal distribution of the specific algal production was present in all simulations (see figure 1 in the appendix). The gross production rate followed the same pattern of horizontal distribution with the maximal growth zone near the surface, except when the phytoplankton was vertically distributed, see plots C_2 , D_2 , G_2 , H_2 , and L_2 in figure 6.

For vertical diffusion coefficients $d_z < 10 \text{ m}^2\text{day}^{-1}$ the model exhibits vertical segmentation of algae and nutrient content, whereas for horizontal diffusion coefficient values above $100 \text{ m}^2\text{day}^{-1}$ horizontal segmentation is present instead provided the diffusion coefficients are not high enough to produce a well mixed system (see plots P_1-P_3). There is thus a transition in behavior from horizontal to vertical distribution when $d_z > d_x$. Note that this behavior is not symmetric around $d_x = d_z$. This is likely due to the fact that the light intensity due to the background light attenuation is only dependent on depth, therefore algae are more prone to segment horizontally if their production is light limited. Additionally, algae will always be light limited at sufficient depths due to the background turbidity which counteracts uniform vertical concentrations, whereas no such mechanism is present for the distribution of nutrients.

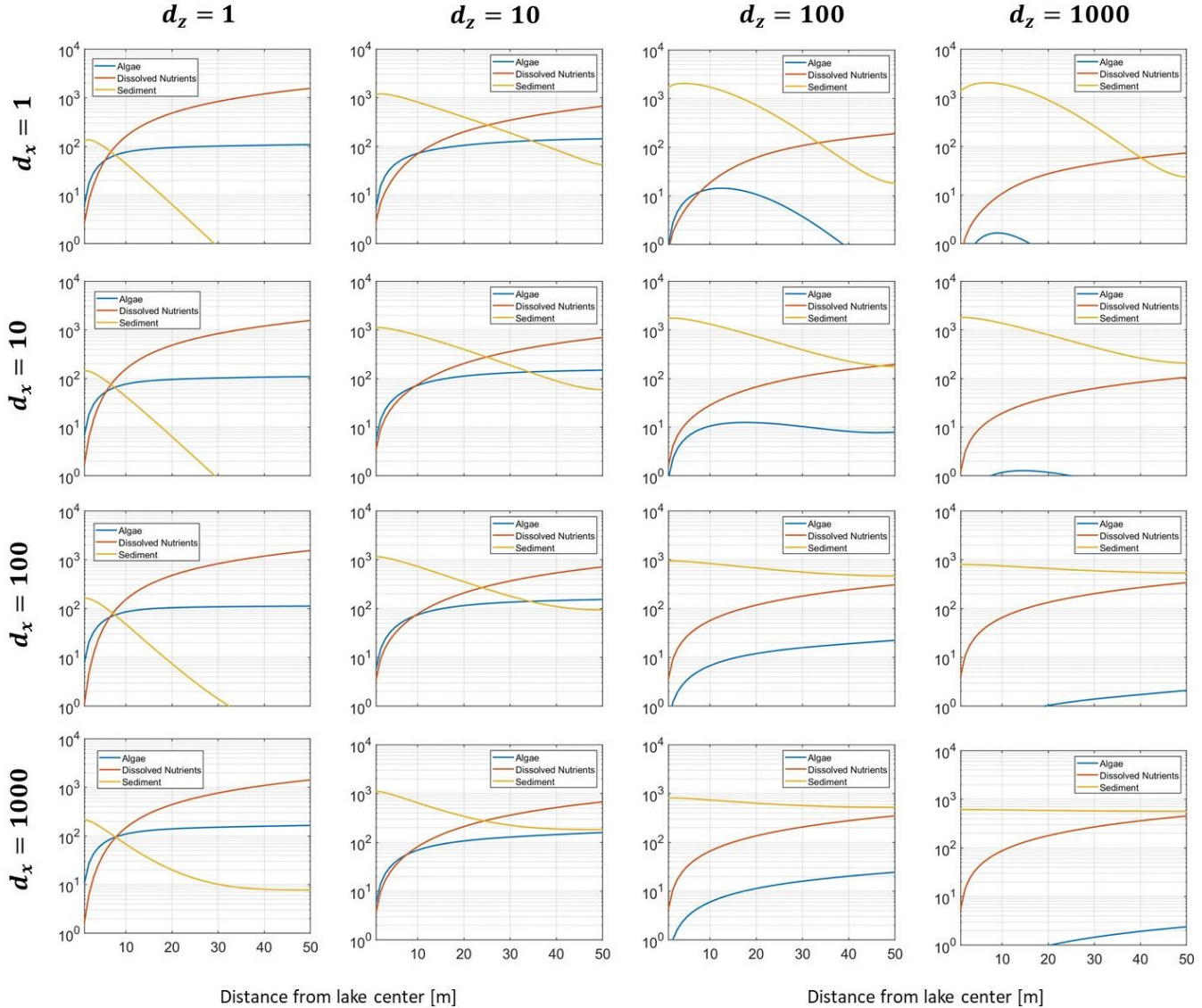


Figure 8: nutrient content of algae, dissolved nutrients, and sediment nutrients integrated over each vertical water column and plotted with a logarithmic y-axis. Sedimented nutrients are colored in yellow, dissolved nutrients in red, and nutrients bound in algae in blue. Note that a common scale is used for all plots to facilitate comparison.

Table 2: Proportion of total nutrients bound in algae.

	$d_z = 1$	10	100	1000
$d_x = 1$	0.1096	0.1288	0.0075	0.0006
10	0.1107	0.1342	.0.0115	0.0010
100	0.1180	0.1377	0.0162	0.0015
1000	0.1631	0.1331	0.0165	0.0015

Table 3: Proportion of total nutrients as dissolved nutrients

	$d_z = 1$	10	100	1000
$d_x = 1$	0.8622	0.3632	0.1083	.0441
10	0.8610	0.3772	.1140	0.0651
100	0.8499	0.3855	0.1877	0.2103
1000	0.7867	0.3762	0.2154	0.2809

Table 4: Proportion of total nutrients bound in sediment

	$d_z = 1$	10	100	1000
$d_x = 1$	0.0282	0.5080	0.8842	0.9553
10	0.0283	0.4886	0.8745	0.9339
100	0.0321	0.4768	0.7961	0.7883
1000	0.0502	0.4907	0.7680	0.7176

5 Discussion

The introduction of a horizontal dimension with independent horizontal diffusion clearly has an affect on phytoplankton dynamics compared to the case with only a vertical dimension. As was discussed in the results section, net plankton biomass is positively correlated to the horizontal diffusion in the explored parameter space (table 2), and increased horizontal diffusion counteracts declines of phytoplankton concentrations at greater depths, phenomena the 1D case studied by Jäger et. al.[26] cannot emulate. However, changes in the proportion of nutrients bound in algae, dissolved nutrients, and sediment was more subtle with varying the horizontal diffusion coefficient d_x compared to d_z (tables 2-4), where clear trends were displayed with varying d_z . This does not exclude the possibility that even small amounts of

horizontal diffusion has a non-negligible effect on plankton dynamics, and the results presented in this thesis is only a first exploration of the dynamics of the model.

5.1 Sediment nutrient concentration

Results indicate that in the parameter space visualized in figure 6, sedimented nutrient concentrations are highest in the shallow regions. In contrast, the opposite is true in real lakes where sediment build up is highest at the bottom of the lake basin [16]. The explanation to this discrepancy lies in multitude of factors that govern sedimentation, some of which are present in the model and some which notably are not.

Where sediment accumulates in the model is governed by the combination of several model parameters. The horizontal and vertical diffusion coefficients govern the diffusive mixing in the lake, and the horizontal diffusion coefficient is especially important because it governs the only mechanism that moves algae and nutrients horizontally. Algae sink vertically, and for low values of the horizontal diffusion coefficient horizontal transport of algae is minimal, and the largest sediment buildup will occur directly below zones of highest productivity which is generally near the shore (see figure 10).

Another factor affecting sediment accumulation is the background respiration losses l_{bg} . This parameter represents all biological processes that result in the loss of nutrients for live algae, including respiration losses and bio-degradation by bacteria. In the model studied in this thesis, algae can only die by respiring away completely or by coming in contact with the bottom and turn into sedimented nutrients. This means that sinking algae will continue to loose biomass and release dissolved nutrients into the water, and if the sinking speed is sufficiently low or the lake is sufficiently deep, they will be completely dissolved before reaching the bottom. This process is also indirectly affected by the horizontal diffusion coefficient, since horizontal movement can transport sinking algae to a shallower depth and thus reach the bottom quicker. This in turn means that at sufficient depths there will be no accumulation nutrients in the sediment at all (assuming the horizontal diffusion coefficient is not high enough to cause horizontal well mixing, i.e. $d_x < 1000m^2 day^{-1}$), because algae will respire away completely into dissolved nutrients before reaching the bottom.

5.2 Finite Volume Method & Alternate Grid

One advantage of using a finite volume method over a finite difference method is that the former can utilize a non Cartesian grid with arbitrarily shaped polygons. The transform used in this thesis was chosen because it would work using a finite difference method which I started out with and it requires a Cartesian computation grid. Unfortunately, after implementing a finite difference solution and discovering that it wasn't conservative, I could prove that it was impossible to satisfy the conservation criteria with the finite difference method I was using, and was forced to change to a finite volume approach.

In hindsight, foregoing the transform altogether would simplify the code allot. Instead of transforming the entire grid, one can instead use a modified Cartesian grid which has been cut in half so that the diagonal elements are triangles, see figure 9 . Calculating the normal of the sloped bottom would then be necessary since it is no longer parallel to the grid axis, but that is trivially easy compared to deriving the expressions for the transform of equations 3 and 4. A finite difference method was used initially to implement the model and finite difference methods require Cartesian computation grids, which is why a non-Cartesian grid was not considered at first. However, the grid used in this thesis has a non-uniform distribution of nodes with a much higher grid refinement at the shore, which can be an advantage since production was consistently high in the shallows (see figure 7).

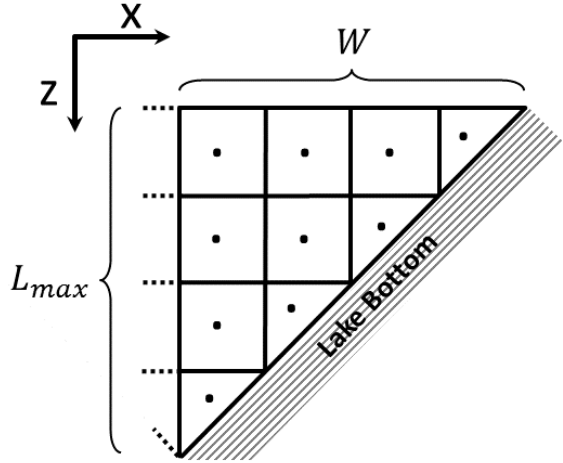


Figure 9: Alternative computation grid, forego-ing the coordinate transform and utilizing a mod-ified Cartesian grid.

5.3 Future Work

First at foremost, before complicating the model further by introducing new dynamics or changing the lake topography substantially, a more thorough exploration of the parameter space of the current model is warranted. For example, algal extinction was not present in the explored parameter space, but with sufficient depth and high enough light attenuation coefficient algae will be severely light limited at greater depths, which will result in local extinction. However, algae from shallower areas can

be transported via sinking and diffusion into areas that are otherwise uninhabitable, which explains the presence of algae everywhere in the lake for all simulations in figure 6, despite that the gross production of the deeper areas was very low (figure 7). For sufficiently low values of the vertical diffusion coefficient, vertical diffusion will be too weak to counteract the downward transport of sinking algae and all algae will come in contact with the bottom and become sedimented nutrients. These nutrients will then remineralize into dissolved nutrients, and the steady state will consist of all nutrients as dissolved nutrients. Simulation attempts were made with small values of the vertical diffusion coefficient, but the method failed to successfully compute an accurate solution due to stiff behavior of the model, see section 3.1. In order to obtain accurate simulations of the model with very low vertical diffusion, the numerical method has to be modified so that it can handle the stiff behavior exhibited in that parameter space.

There are several directions in which one can extend the model studied in this thesis. One natural first step would be to study the effect a non-linear bottom has on algal growth, and compare results to the linear case. Since the transform is defined with a parameter α for the slope, one can precisely specify the curvature of the bottom. This allows for a non-linear distribution of depths, and a question one might ask is if this new scenario with a non-linearly sloping bottom is equivalent to some linear case, or is the dynamics introduced by a non-linear slope unique? Alternatively, one can ask the question if there is some way to approximate the 2D results with the original 1D model by Jäger et. al.[26], perhaps by averaging results from separate simulations with varying depths corresponding to the geometry of the 2D case. If this is possible, the introduced second dimension might be superfluous if spacial distributions are not of interest.

One assumption made in the model is the negligible thickness of the sediment layer. In real lakes, sediment buildup at the bottom fills lake gradually until they disappear completely, a process called sediment burial. This is generally a slow process, for example the ancient Lake Tanganyika in Tanzania displays sedimentation rates of 0.3 mm year^{-1} [27]. However, man-made bodies of water with poorly vegetated catchments displaying rich concentrations of nutrients, a property called eutrophication [8], can exhibit sedimentation rates of $> 40 \text{ cm year}^{-1}$. In all lakes only the topmost parts of the sediment layer is in active exchange with the rest of the lake, because the organisms that live in the sediment require oxygen for respiration and the oxygen concentration in the sediment rapidly decreases with depth. This results in a burial effect of nutrients in the sediment, and the sediment can thus be seen as a sink that seals away nutrients with time. For example Lake Tanganyika has a sediment layer in excess of 6000 m deep, which has been building up contin-

uously since its formation 9-12 million years ago [44]. There are several approaches to modelling sediment burial depending on the desired simulation timescales. The simplest approach would be to introduce a constant burial rate from the sediment layer, where nutrients are continuously removed from the sediment. Alternatively the burial could depend on the local influx of the nutrients, such that more burial takes place in areas where there is a high sediment deposition. If the timescales are long enough such that sedimentation burial has a significant effect on lake depth, the model has to take this into account to avoid non-negligible errors. This results in a non-stationary bottom boundary that depends on the local burial of nutrients, and is a significantly harder challenge to model compared to a simple linear burial with constant borders.

One can also replace the constant diffusion coefficients with spatially dependent functions. this allows for depth dependent diffusion that enables the model to replicate the real life phenomenon of high turbulence at the surface due to heat transfer from the atmosphere and wind, and low turbulence at the bottom due to uniform temperatures and little or no physical mechanisms increasing turbulence [28]. The current model does not take into account daily and seasonal changes, and the incoming light intensity is constant. Adding a 24h light cycle and especially seasonal changes to the incoming light is an option of model refinement which could introduce interesting new dynamics. For example, the presence of surface ice has a major impact on phytoplankton abundance in lakes, with a reduction of mean phytoplankton and zooplankton biomass in excess of 50% in comparison to summer values [17]. Note that seasonality and ice formation are mechanisms that influence the turbidity of the lake and thus affect the diffusion coefficients, which would need to be modelled to emulate the effects of changing seasons.

The current model assumes uniformity in the omitted horizontal dimension, and the geometry can be seen as a cross-section of a rectangular lake with a sloping bottom, similar to a rectangular swimming pool with a deep end and a shallow end. However, a circular lake would be a better approximation of the geometry of real lakes, and one can implement this by using cylindrical coordinates instead of Cartesian coordinates. In the reduced 2D case studied in this thesis, this will result in a horizontal diffusion coefficient that is dependent on the distance from the center of the lake, where diffusion is highest at the center and lowest at the edge. The intuition behind this is that if a particle is situated in the center of the lake, any movement in the horizontal plane will result in a change of the radial component of the particles cylindrical coordinates. but if the particle is not at the center, it can move perpendicular to the radial direction (along the azimuth) and its radial component is unchanged even though the particle has moved.

The ecological scope and detail of the model can be extended in several directions. Constraining the model to primary producers, adding benthic algae which live attached to the lake bottom would introduce potentially interesting dynamics, where a resource tug of war would result between the free floating phytoplankton who have access to more light than the benthic algae below, whereas the benthic algae has immediate access to the nutrients in the sediment layer. This would be a continuation of the work by Jäger & Diehl [25] who modelled phytoplankton and benthic algae in 1D with the reaction-advection-diffusion equation. Adding a second spatial dimension means that the benthic algae will always have access to lake bottom strata at shallow depths, potentially introducing new dynamics not present in the 1D case and more closely mimicking real world scenarios. The model is not limited to primary producers however, and can be extended to include single animal species, or indeed an entire ecosystem with grazers, omnivores and carnivores. Adding additional species to the model is relatively straight forward, however the introduced dynamics are potentially very complicated and one has to carefully consider what the intention of the model extension is before adding more detail.

6 Conclusion

In this thesis the phytoplankton model by Jäger et. al. [26] was extended to two dimensions using a cell centered finite volume method. In order to compare the dynamics of the 2D model with the 1D results presented by [26], The lake geometry was devised such that the depth varied linearly, diffusion coefficients in the x and z direction where varied independently of each other and the model was run to steady state with the same parameter values as [26]. Results indicate that the introduction of a horizontal dimension results in the survival of phytoplankton in the explored parameter space, in contrast to the observation by Jäger et. al. where plankton extinction sometimes took place at greater depths. Results presented in this thesis is only a first exploration of the dynamics of the model, and a more extensive exploration of the parameter space is necessary to fully understand how observed behavior generalises. Horizontal movement and access to varying depths introduces interesting dynamics in the model, and the door is open to a myriad of extensions such as introducing additional parts of lake ecosystems such as benthic algae, grazers, and fish, or abiotic factors such as seasonality, external nutrient influx, and more complex lake geometries.

References

- [1] UNEP. (2014). Using Models for Green Economy Policymaking.
- [2] Andrew J. Black and Alan J. McKane. Stochastic formulation of ecological models and their applications. *Trends in Ecology & Evolution*, 27(6):337 – 345, 2012.
- [3] Paul-Marie Boulanger and Thierry Bréchet. Models for policy-making in sustainable development: The state of the art and perspectives for research. *Ecological Economics*, 55(3):337 – 350, 2005.
- [4] BAM Bouman. Linking physical remote sensing models with crop growth simulation models, applied for sugar beet. *International Journal of Remote Sensing*, 13(14):2565–2581, 1992.
- [5] Larry E. Brand. The salinity tolerance of forty-six marine phytoplankton isolates. *Estuarine, Coastal and Shelf Science*, 18(5):543 – 556, 1984.
- [6] T.D. Bui and T.R. Bui. Numerical methods for extremely stiff systems of ordinary differential equations. *Applied Mathematical Modelling*, 3(5):355 – 358, 1979.
- [7] Albert Calbet and Michael R. Landry. Phytoplankton growth, microzooplankton grazing, and carbon cycling in marine systems. *Limnology and Oceanography*, 49(1):51–57, 2004.
- [8] Michael F Chislock, Enrique Doster, Rachel A Zitomer, and AE Wilson. Eutrophication: causes, consequences, and controls in aquatic ecosystems. *Nature Education Knowledge*, 4(4):10, 2013.
- [9] J. K. Egge and D. L. Aksnes. Silicate as regulating nutrient in phytoplankton competition. *Marine Ecology Progress Series*, 83(2/3):281–289, 1992.
- [10] J. A. Elliott, I. D. Jones, and S. J. Thackeray. Testing the sensitivity of phytoplankton communities to changes in water temperature and nutrient load, in a temperate lake. *Hydrobiologia*, 559(1):401–411, Apr 2006.
- [11] Paul G. Falkowski. Rationalizing elemental ratios in unicellular algae. *Journal of Phycology*, 36(1):3–6, 2000.
- [12] Adolf Fick. Ueber diffusion. *Annalen der Physik*, 170(1):59–86, 1855.

- [13] Christopher B. Field, Michael J. Behrenfeld, James T. Randerson, and Paul Falkowski. Primary production of the biosphere: Integrating terrestrial and oceanic components. *Science*, 281(5374):237–240, Jul 10 1998. Copyright - Copyright American Association for the Advancement of Science Jul 10, 1998; Last updated - 2017-10-31; CODEN - SCIEAS.
- [14] Thomas R. Fisher, Emily R. Peele, James W. Ammerman, and Lawrence W. Harding. Nutrient limitation of phytoplankton in chesapeake bay. *Marine Ecology Progress Series*, 82(1):51–63, 1992.
- [15] Jennifer S Ford and Ransom A Myers. A global assessment of salmon aquaculture impacts on wild salmonids. *PLOS Biology*, 6(2):1–7, 02 2008.
- [16] Lars Håkanson. *Lakes: form and function*. Blackburn Press Caldwell, New Jersey, 2004.
- [17] Hampton and Stephanie E 61 co authors. Ecology under lake ice. *Ecology Letters*, 20(1):98–111, 2017.
- [18] Lars-Anders Hansson. *The Biology of Lakes and Ponds*. Oxford University Press, 2005.
- [19] P. J. Harrison, P. A. Thompson, and G. S. Calderwood. Effects of nutrient and light limitation on the biochemical composition of phytoplankton. *Journal of Applied Phycology*, 2(1):45–56, Mar 1990.
- [20] R. E. Hecky and P. Kilham. Nutrient limitation of phytoplankton in fresh-water and marine environments: A review of recent evidence on the effects of enrichment. *Limnology and Oceanography*, 33(4part2):796–822, 1988.
- [21] William G Hecky. Interrelated influence of iron, light and cell size on marine phytoplankton growth. *Nature*, 390:389–392, 1997.
- [22] Kjetil Hindar, Ian A. Fleming, Philip McGinnity, and Ola Diserud. Genetic and ecological effects of salmon farming on wild salmon: modelling from experimental results. *ICES Journal of Marine Science*, 63(7):1234–1247, 10 2006.
- [23] Gilles Horowitz. Drift-diffusion current in organic diodes. *Bulletin of Mathematical Biology*, 79(4):693–737, 2017.
- [24] Michael A. Huston and Steve Wolverton. The global distribution of net primary production: resolving the paradox. *Ecological Monographs*, 79(3):343–377, 2009.

- [25] Christoph G. Jäger and Sebastian Diehl. Resource competition across habitat boundaries: asymmetric interactions between benthic and pelagic producers. *Ecological Monographs*, 84(2):287–302, 2014.
- [26] Christoph G. Jäger, Sebastian Diehl, and Maximilian Emans. Physical determinants of phytoplankton production, algal stoichiometry, and vertical nutrient fluxes. *The American Naturalist*, 175(4):E91–E104, 2010. PMID: 20178423.
- [27] Jacob Kalf. *Limnology: Inland Water Ecosystems*. Prentice-Hall, Upper Saddle River, NJ 07458, 2002.
- [28] G. Kirillin and T. Shatwell. Generalized scaling of seasonal thermal stratification in lakes. *Earth-Science Reviews*, 161:179 – 190, 2016.
- [29] R Lindsey and M Scott. What are phytoplankton? <https://earthobservatory.nasa.gov/features/Phytoplankton>. Accessed: 2019-05-23.
- [30] Christopher V. Manhard, Nicholas A. Som, Russell W. Perry, and John M. Plumb. A laboratory-calibrated model of coho salmon growth with utility for ecological analyses. *Canadian Journal of Fisheries and Aquatic Sciences*, 75(5):682–690, 2018.
- [31] Amy M Marcarelli, Wayne A Wurtsbaugh, and Olivia Griset. Salinity controls phytoplankton response to nutrient enrichment in the great salt lake, utah, usa. *Canadian Journal of Fisheries and Aquatic Sciences*, 63(10):2236–2248, 2006.
- [32] John H. Martin. Iron deficiency limits phytoplankton growth in the north-east pacific subarctic. *Nature*, 331:341–343, 1988.
- [33] Yuxin Miao, David J Mulla, William D Batchelor, Joel O Paz, Pierre C Robert, and Matt Wiebers. Evaluating management zone optimal nitrogen rates with a crop growth model. *Agronomy Journal*, 98(3):545–553, 2006.
- [34] Jacques Monod. The growth of bacterial cultures. *Annual Review of Microbiology*, 3(1):371–394, 1949.
- [35] Cesare Pacini, Ada Wossink, Gerard Giesen, and Ruud Huirne. Ecological-economic modelling to support multi-objective policy making: a farming systems approach implemented for tuscany. *Agriculture, Ecosystems & Environment*, 102(3):349–364, 2004.

- [36] E. M. Pankratova. Functioning of cyanobacteria in soil ecosystems. *Eurasian Soil Science*, 39(1):S118–S127, Dec 2006.
- [37] Mads Lund Pedersen, Michael J. Frank, and Guido Biele. The drift diffusion model as the choice rule in reinforcement learning. *Psychonomic Bulletin & Review*, 24(4), Aug 2017.
- [38] Robert Ptacnik, Angelo G. Solimini, Tom Andersen, Timo Tamminen, Pål Brettmann, Liisa Lepistö, Eva Willén, and Seppo Rekolainen. Diversity predicts stability and resource use efficiency in natural phytoplankton communities. *Proceedings of the National Academy of Sciences*, 105(13):5134–5138, 2008.
- [39] Drew Purves, Jörn PW Scharlemann, Mike Harfoot, Tim Newbold, Derek P Tittensor, Jon Hutton, and Stephen Emmott. Ecosystems: time to model all life on earth. *Nature*, 493(7432):295, 2013.
- [40] S. Z. Qasim, P. M. A. Bhattathiri, and V. P. Devassy. The influence of salinity on the rate of photosynthesis and abundance of some tropical phytoplankton. *Marine Biology*, 12(3):200–206, Feb 1972.
- [41] W.E. Ricker. Stock and recruitment. *Journal of the Fisheries Research*, 11(1):559–623, 1954.
- [42] J. P. Riley and Igal Roth. The distribution of trace elements in some species of phytoplankton grown in culture. *Journal of the Marine Biological Association of the United Kingdom*, 51(1):63–72, 1971.
- [43] Amelie Schmolke, Pernille Thorbek, Donald L. DeAngelis, and Volker Grimm. Ecological models supporting environmental decision making: a strategy for the future. *Trends in Ecology & Evolution*, 25(8):479 – 486, 2010.
- [44] Christopher A Scholz and BR Rosendahl. Low lake stands in lakes malawi and tanganyika, east africa, delineated with multifold seismic data. *Science*, 240(4859):1645–1648, 1988.
- [45] Swinehart. The beer-lambert law. *Journal of Chemical Education*, 39(7):333–335, 1962.
- [46] Heather M Tallis and Peter Kareiva. Shaping global environmental decisions using socio-ecological models. *Trends in Ecology & Evolution*, 21(10):562–568, 2006.

- [47] Jeroen CJM Van den Bergh and Peter Nijkamp. Operationalizing sustainable development: dynamic ecological economic models. *Ecological Economics*, 4(1):11–33, 1991.
- [48] Jana Verboom, Rob Alkemade, Jan Klijn, Marc J Metzger, and Rien Reijnen. Combining biodiversity modeling with political and economic development scenarios for 25 eu countries. *Ecological economics*, 62(2):267–276, 2007.
- [49] Kenneth Wertheim and Tiina Roose. A mathematical model of lymphangiogenesis in a zebrafish embryo. *Bulletin of Mathematical Biology*, 79(4):693–737, 2017.
- [50] Hai Xu, Hans W. Paerl, Boqiang Qin, Guangwei Zhu, and Guang Gaoa. Nitrogen and phosphorus inputs control phytoplankton growth in eutrophic lake taihu, china. *Limnology and Oceanography*, 55(1):420–432, 2010.

A Specific production and gross production

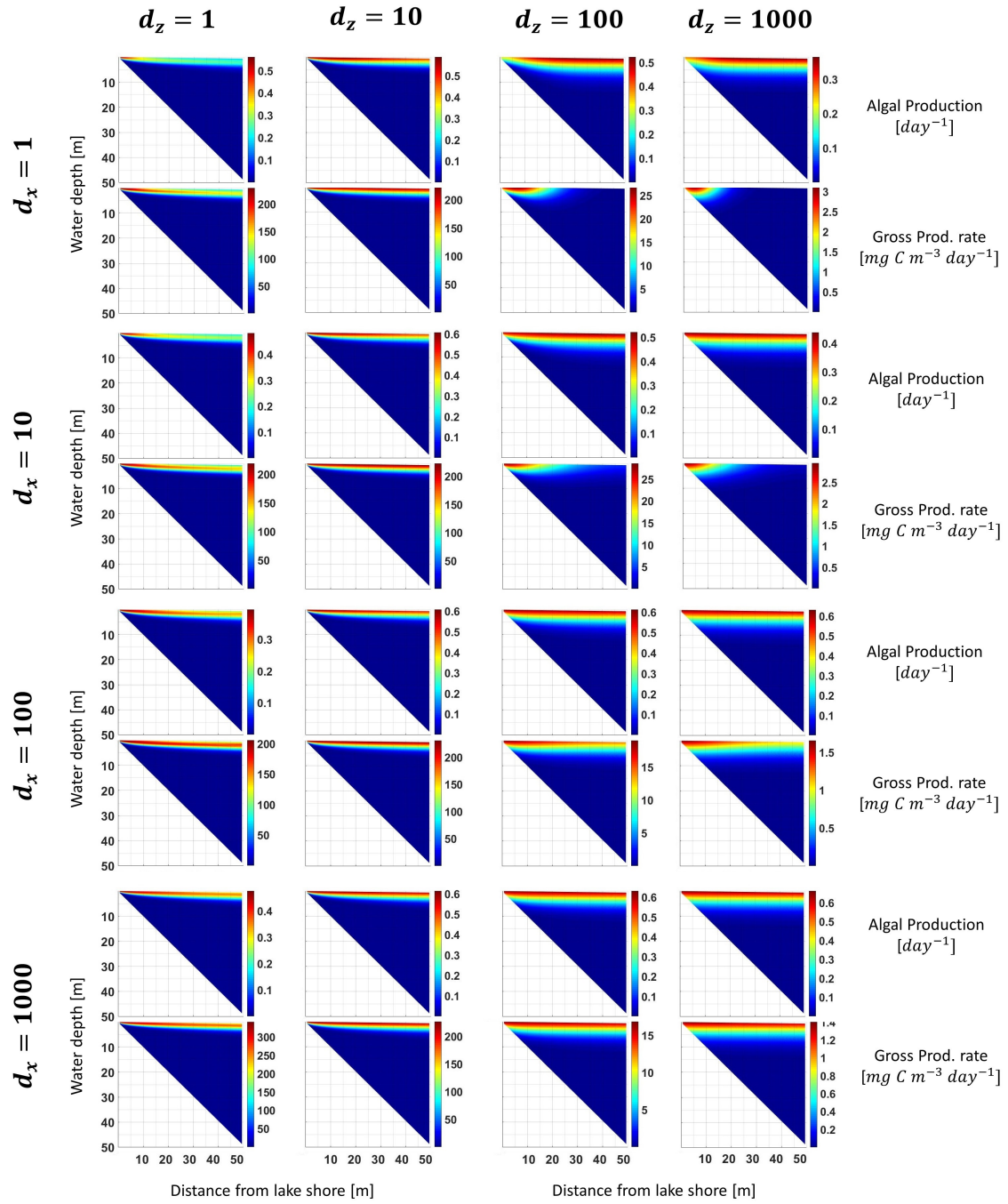


Figure 10: Algal production and gross production rate at steady state for varying diffusion coefficients. All parameters where kept constant except the diffusion coefficients, see table 1 for numerical values. The x-axes corresponds to the distance from the lake center (right border), and the y-axis corresponds to water depth. The diffusion coefficients where varied independently with values 1, 10, 100, and $1000 \text{ m}^2\text{day}^{-1}$. The plots are grouped and numbered such that X_1 is the nutrient content in the sediment, X_2 is the nutrient concentration bound in algae, and all plots X_n correspond to the same set of parameters. Note that the color bars are scaled individually for each plot, so while the same qualitative pattern is present in both H_2 and C_2 for example, the concentration of nutrient in C_2 is much higher.